Non-Fluorinated Proton Exchange Membranes Based on Melt Extruded SEBS/HDPE Blends

Mokrini, Asmae; Huneault, Michel; Shi, Zhiqing; Xie, Zhong; Holdcroft, Steven

Publisher's version / Version de l'éditeur:
https://doi.org/10.1016/j.memsci.2008.08.051
Journal of Membrane Science, 325, December 2, pp. 749-757, 2008

Journal of Membrane Science 325 (2008) 749–757

Contents lists available at ScienceDirect

Journal of Membrane Science

journal homepage: www.elsevier.com/locate/memsci

Non-fluorinated proton-exchange membranes based on melt extruded SEBS/HDPE blends

Asmae Mokrini[a,*], Michel A. Huneault[a], Zhiqing Shi[b], Zhong Xie[b], Steven Holdcroft[b]

[a] Industrial Materials Institute, National Research Council, 75 de Mortagne, Boucherville, Quebec J4B 6Y4, Canada
[b] Institute for Fuel Cell Innovation, National Research Council Canada, 4250 Wesbrook Mall, Vancouver, British Columbia V6T 1W5, Canada

ARTICLE INFO

Article history:
Received 22 May 2008
Received in revised form 28 August 2008
Accepted 29 August 2008
Available online 16 September 2008

Keywords:
Proton-exchange membrane
Melt-extrusion
HDPE
SEBS

ABSTRACT

This paper reports on functional polymer blends prepared by melt-processing technologies for proton-exchange membrane applications. Styrene–ethylene/butylene–styrene (SEBS) and high-density polyethylene (HDPE) were melt blended using twin-screw compounding, extruded into thin films by extrusion–calendering. The films were then grafted with sulfonic acid moieties to obtain ionic conductivity leading to proton-exchange membranes. The effect of blend composition and sulfonation time was investigated. The samples were characterized in terms of morphology, microstructure, thermo-mechanical properties and in terms of their conductivity, ion exchange capacity (IEC) and water uptake in an effort to relate the blend microstructure to the membrane properties. The HDPE was found to be present in the form of elongated structures which created an anisotropic structure especially at lower concentrations. The HDPE increased the membrane mechanical properties and restricted swelling, water uptake and methanol crossover. Room temperature through-plane conductivities of the investigated membranes were up to 4.5E−02 S cm^{-1} at 100% relative humidity, with an ionic exchange capacity of 1.63 meq g^{-1}.

1. Introduction

Proton-exchange membrane fuel cells (PEMFC) are one of the most attractive power sources for a wide variety of applications, ranging from vehicles to portable devices, due to its inherently high efficiency and low emission. Hydrogen fuel cells have the highest performance, however, the use of hydrogen brings issues regarding the appropriate generation, safe transportation and storage of the fuel. Consequently, direct methanol fuel cells (DMFC) that can directly utilize a liquid fuel, without reforming, is attractive [1–3]. Despite its advantages, there are several obstacles preventing large-scale commercialization of DMFC. The main issue is the non-availability of a suitable proton-conducting membrane due to the unacceptably high methanol crossover of currently used perfluorosulfonic acid membranes. The majority of polymer electrolytes used successfully in the hydrogen fuel cells, such as Nafion® (DuPont) is too permeable to methanol and thus cannot be utilized in direct methanol fuel cells due to excessive fuel crossover. High crossover rates have a harmful effect on DMFC performance because it cause performance loss at the cathode due to the catalyst poisoning that reduces its ability to efficiently reduce oxygen, and as a consequence reduces the overall energetic efficiency of the fuel cell [4,5]. These disadvantages and the demand for cost efficient materials, have driven academia, government and industry to focus on new alternative PEM materials that do not rely on expensive, fully fluorinated polymers.

Sulfonated polystyrene-based polymers (sPS) were the first hydrocarbon-based membranes used as electrolytes in PEMFC in the early 1960s. However, hydrogen PEMFCs using these membranes showed poor performance and short lifetime. The main drawback in employing sPS and hydrocarbon-based materials in general, was their poor chemical stability compared to perfluorinated or partially perfluorinated membranes [6]. However, hydrocarbon-based membranes are promising candidates for direct methanol fuel cells DMFC, because of their potential for lowering cost and methanol permeability.

The chemical stability and performance of hydrocarbon-based membranes has been thoroughly investigated [7]. Chemically grafted polymers have received attention for the fabrication of electrolyte membranes due to their low cost and to the variety of functional groups that can be used. Films of poly(vinylidene fluoride) PVDF, poly(vinylidene fluoride-co-hexafluoropropylene) PVDF-co-HFP, poly(ethylene–tetrafluoroethylene) ETFE, poly (tetrafluoroethylene-co-hexafluoropropylene) FEP or low-density polyethylene LDPE have been used as base polymer for membrane fabrication [8–12]. These films were radiation grafted with styrene or styrene derivatives such as m,p-methylstyrene or

* Corresponding author. Tel.: +1 450 641 5024.
E-mail address: Asmae.mokrini@cnrc-nrc.gc.ca (A. Mokrini).

0376-7388/$ – see front matter.
doi:10.1016/j.memsci.2008.08.051

p-tert-butylstyrene [13], and subsequently sulfonated to attain high proton conductivity. It has been demonstrated that sPS-g-FEP based membranes shows very high stability, over 2500 h, in a H_2/O_2 fuel cell [14].

Organic/inorganic composite membranes have also been used widely to decrease methanol permeation [15]. Generally, inorganic fillers must be proton conducting, such that methanol permeation is decreased without overly compromising proton conductivity. The inorganic proton-conducting moieties that have been considered range from weakly acidic silica [16] and neutral titanium oxides [17] and clays [18], through common acids such as phosphoric acids, to super acids such as the heteropolyacids [19] and zirconium phosphonates [20].

Polymer blending is another alternative in the development of better polyelectrolyte chemistry [21–23]. Blends of proton-conducting and non-proton-conducting polymer pairs, can be used to take advantages of either interfacial or geometrical synergistic effects of polymer–polymer interactions. Carefully selected blend morphologies could improve methanol fuel cell performance by restricting, for example, the swelling of the hydrophilic blend component in such a way that the benefit in methanol crossover reduction is far greater than the drawback related to proton conductivity reduction. Recent investigations on the fabrication of polymer blend membranes produced using melt-processing technologies have shown the potential of this approach [24–26]. The use of melt-processable polymers provides a significant cost-reduction compared to conventional PEM fabrication technologies and simplifies the scale-up toward mass production. Furthermore, the degree of crystallinity reached for extruded polymers is greater than that obtained using solvent-casting methods leading to improved mechanical strength and durability of polymer membranes. The blends studied in this paper are based on poly(styrene–(ethylene–butylene)–styrene) triblock copolymer (SEBS) and high-density polyethylene (HDPE). SEBS is a commercially available thermoplastic elastomer. The styrene blocks of the SEBS can be subsequently sulfonated providing high ionic conductivity [27–31]. The membranes based on sulfonated SEBS (s-SEBS) are reported to be less expensive to produce than Nafion®. They also exhibit a rich array of microphase separated morphologies [32]. However, like fluorinated polymers, s-SEBS membranes are prone to methanol crossover [33]. The addition of HDPE to s-SEBS can partially circumvent this drawback since HDPE is a good barrier to methanol and to other polar solvents. In addition, HDPE is a highly crystalline and chemically resistant polymer that can infer good dimensional stability and mechanical resistance to the membranes.

In this study we will investigate the use of polymer blending as a route to tailor the membrane properties to specific performance profiles for the DMFC applications. Twin-screw extrusion process was used to produce SEBS/HDPE blends with a HDPE content ranging from 30 to 60 wt.% and thin films were formed by calendering. Membranes were obtained by functionalizing the films by solid-state sulfonation. The membranes were then characterized in terms of their microstructure, mechanical properties, conductivity, ion exchange capacity (IEC), water uptake and stability in an oxidizing environment, to establish the structure–property relationships.

2. Experimental

2.1. Materials

Polymers used in this study were \high-density polyethylene and styrene–(ethylene–butylene)–styrene triblock copolymer. The HDPE grade was HDPE 1000 supplied by Petromont. The SEBS grade, G1652 supplied Kraton Polymers contained 30 wt.% styrene and has an average molecular weight M_w = 125,000. Chlorosulfonic acid, dichloroethane (DCE), dimethylacetamide (DMAc), methanol, sodium chloride, sodium hydroxide, phenolphthalein, potassium permanganate, sulfuric acid and orthophosphoric acid were supplied by Aldrich Chemicals and used as received.

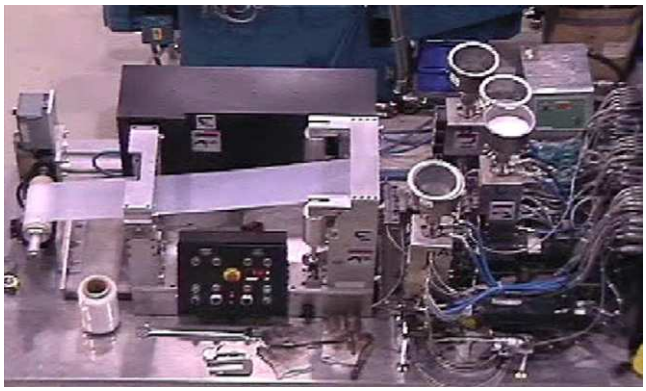

Fig. 1. Randcastle extrusion film line used for membranes forming.

2.2. Membranes fabrication

Membranes were prepared in a three-step process. First, blends comprising 30, 40, 50 and 60 wt.% of HDPE were compounded at 230 °C on a ZSK-30 mm co-rotating twin-screw extruder operated at a throughput rate of 5 kg/h and using screw rotation speed of 15.7 rad/s (150 rpm). The extruded strands were quenched in water, cut into granules and dried 24 h in an oven at 80 °C prior to film extrusion–calendering. The second step consisted in forming thin films using a 12 mm Randcastle vertical single-screw extruder equipped with a 200 mm wide sheet die (Fig. 1). The extrusion line was operated at 230 °C and at a rotation speed of 10.5 rad/s (100 rpm). The sheet die gap was set to 0.5 mm. The sheets were stretched in machine direction and calendared with rolls maintained at 70 °C and operated at a linear speed of 0.5 cm/min to achieve 150–200 μm thick films. The third step was the film functionalization using chlorosulfonic acid to obtain proton-exchange membranes. Samples were immersed in a solution of chlorosulfonic acid ($ClSO_3H$) in 1,2-dichloroethane (DCE) at room temperature. The $ClSO_3H$ concentration was 0.75 M as this concentration was high enough to maintain acid concentration constant during sulfonation. Sulfonation time was varied from 60 to 120 min to obtain proton-exchange membranes with different ionic exchange capacities. The volume of the sulfonation solution was kept constant in relation to the mass of the film to be sulfonated. The sulfonation reaction was terminated by soaking the films during 1 h in methanol at room temperature and 1 h in a mixture 1:1 methanol:deionised water at 80 °C. They were finally washed several times and stored in the acid form in deionised water. The procedure has been described previously in greater details [24].

2.3. Blend membranes characterization

2.3.1. Blend morphology

Blend morphology was determined using scanning electron microscopy (SEM) and atomic force microscopy (AFM). For SEM, strands extruded by the twin-screw extrusion process and membranes prepared by calendaring were microtomed in the machine direction (MD) or perpendicular to the extrusion direction (TD). The details of the crystalline morphology were, enhanced by selectively etching the amorphous domains using a solution of 0.7 wt.%/v potassium permanganate in a 2:1 mixture of sulfuric and

orthophosphoric acids according to the procedure of Olley et al. [34]. The SEM analysis was carried out on the platinum-sputtered surfaces at a 1 kV acceleration voltage.

For AFM analysis, samples were microtomed at −100 °C and examined without further treatment. Tapping mode was used at 300 kHz frequency and good contrast was found between amorphous and crystalline phases as they exhibit very different surface properties.

2.3.2. Thermal analysis

Differential Scanning Calorimetry (DSC) was used to determine the thermal transitions of the blends. Samples were first cooled to −90 °C, and scanned from −90 to 250 °C to determine glass transition and melting temperatures and from 250 to −90 °C to determine the crystallization temperature. The heating/cooling rate used was 20 °C/min. The crystallinity of HDPE in the samples was determined from the area under the melting peak, assuming a heat of fusion of $\Delta H_m^0 = 280 j/g$ for HDPE. Dynamic Mechanical Thermal Analysis (DMTA) was used to measure the glass transition temperatures (T_g) for the pure SEBS and its blends since these transitions were not clearly visible on the DSC thermograms. A Rheometric Scientific dynamic mechanical thermal analyzer (DMTA) model V was used. The films were cut into rectangular samples of approximately 27 mm × 5 mm. The measurements were performed in a multi-frequency single cantilever mode at 1 Hz frequency using rectangular tension/compression geometry, with a target strain of 0.1%. Samples were heated using a dynamic temperature ramp from −100 to 130 °C at a heating rate of 2 °C/min.

2.3.3. Mechanical properties

Tensile mechanical properties of films were measured according to standard ASTM D882. The test specimens consisted of 19 mm × 150 mm strips. The gage length used was 50 mm. The samples were drawn at 500 mm/min. Each reported value is the average of five measurements.

2.3.4. Ion exchange capacity and degree of sulfonation

Once the polymer films were functionalized with chlorosulfonic acid, their electrochemical properties were measured. First, the ion exchange capacity was determined by equilibrating the membranes for at least 24 h in NaCl (0.2 M) at room temperature with occasional agitation. Aliquots of exchanged solutions were then titrated with NaOH (0.005 M) to the phenolphthalein end point. The procedure was carried out in triplicate and the results averaged. Degree of sulfonation (DS) was calculated from experimental IEC and of 100% is defined as an ion-exchange capacity equivalent to one $–SO_3H$ group per aromatic ring according to the formula:

$$\mathrm{DS}\,(\%) = \left(\frac{\mathrm{IEC_{exp}}}{\mathrm{IEC_{Theor}}}\right) \times 100$$

where $\mathrm{IEC_{exp}}$ is the ion exchange capacity determined by titration and $\mathrm{IEC_{Theor}}$ is the ion exchange capacity calculated considering 100% sulfonation of styrene groups of SEBS. A degree of sulfonation of 100% is defined as an IEC equivalent to one $–SO_3H$ group per aromatic ring.

2.3.5. Equilibrium water content

The water content was determined by equilibrating the membranes in deionised water at room temperature. They were then removed from the water container, quickly dry wiped and immediately weighed. Subsequently, they were dried to weight constancy under vacuum at room temperature and again weighed. The water content is calculated from the weight difference of the membrane in its hydrated and dry state [25], according to the following equation:

$$\mathrm{WC}\,(\%) = \left(\frac{m_{\mathrm{wet}} - m_{\mathrm{dry}}}{m_{\mathrm{wet}}}\right) \times 100 \quad (1)$$

where m_{wet} is the weight of the hydrated membrane, and m_{dry} is its dry weight. Three measurements were carried out for each membrane.

2.3.6. Proton conductivity

Electrochemical impedance spectroscopy (EIS) was used to measure ionic conductivity of the membrane. For a first screening, measurements were done at ambient temperature and 100% relative humidity (RH). Samples were sandwiched between blocking electrodes using a through-plane conductivity cell and measured using a HP4192A impedance analyzer. Scans were carried out in the 50 kHz to 13 MHz frequency range with a 0.1 V applied AC signal. A Nafion112® sample was measured as a reference before each series of measurements. As commonly accepted, the resistivity of the membrane was evaluated from the high frequency part of the Nyquist plot that coincides with the bulk resistance of the polymer [25]. Ionic conductivity of the samples were calculated using the following equation:

$$\sigma = \frac{1}{R_{\mathrm{b}}} \cdot \frac{d}{S} \quad (2)$$

where σ is the conductivity ($\Omega^{-1}\,\mathrm{cm}^{-1}$), d is the distance between electrodes (cm), S is the contact area between the electrodes and the polymer film (cm^2), and R_{b} is the bulk resistance calculated from Nyquist plots (Ω).

For conductivity measurements under conditions of variable temperature and relative humidity, the samples were placed in an ESPEC SH-240 temperature/humidity chamber. The proton conductivity was measured using a two-point probe in-plane conductivity cell and a Solartron 1260 with a frequency range of 100 kHz to 10 MHz.

The activation energies (E_{a}) were obtained from the slopes of the Arrhenius plots according to Eq. (3):

$$\sigma = \sigma_0 \exp\left(-\frac{E_{\mathrm{a}}}{RT}\right) \quad (3)$$

2.3.7. Thermal stability

The thermal stability of the PEM materials was investigated using a Setaram TG96 thermogravimetric analyzer. The weight loss and thermal properties were probed simultaneously using a combined TGA–DTA technique. Samples were dried under vacuum overnight to remove any free-water from the samples prior to testing. The thermograms were obtained from 25 to 400 °C at a heating rate of 5 °C/min under an oxygen atmosphere.

2.3.8. Methanol crossover

Methanol crossover was measure by performing choronoamperometry on 5 cm^2 MEAs prepared in the following manner. Catalyst ink was sprayed onto carbon paper (Toray-TGP60, 10% wet-proofed. The anode contained 4 $\mathrm{mg/cm}^2$ of catalyst (40 wt.% Pt-Ru (1:1)/C) and 20 wt.% Nafion®. The cathode contained 0.5 $\mathrm{mg/cm}^2$ catalyst (20 wt.% Pt/C), and 30 wt.% Nafion®. Membrane-electrode assemblies were hot-pressed at 135 °C/226.8 kg (500 pound) for 2 min. Anode was supplied with 1 M MeOH (5 cm^3/min) and used as the reference and counter electrode, while the cathode was supplied with dry nitrogen (100 cm^3/min). The flux of methanol permeating the membrane was measured by choronoamperometry with a potential step of 200 mV vs. reference electrode at 30 and 60 °C.

3. Results and discussion

3.1. Morphological and thermo-mechanical analysis

HDPE and SEBS are immiscible but they form a relatively compatible polymer pair in the sense that the components readily form finely segregated dual-phase morphology due to low interfacial tension and that the two materials show good adhesion in the solid-state. For the membrane application, a continuous network of a proton-conducting phase within the material is essential. In the current system, SEBS must therefore form the matrix while the HDPE must form the dispersed phase or in the limiting case could form a co-continuous network. The shape of dispersed HDPE phase is expected to play a critical role on the mechanical integrity and hydro-mechanical stability of the films, which in turn will have a significant impact on the functional properties of the membrane.

SEM micrographs of a 50:50 SEBS/HDPE blend are presented in Fig. 2. The cryogenically fractured surface, presented in Fig. 2a, showed a smooth surface with no sign of interfacial delamination between components. This is typical of a highly compatible blend and is indicative of the good interfacial adhesion. Since it was difficult to selectively extract HDPE without affecting the SEBS matrix, microtomed samples were selectively etched to remove amorphous phases and create a contrast between crystalline and amorphous phases. Fig. 2b and c present the SEM micrographs obtained after etching at two different magnifications. The lighter areas are the crystalline HDPE domains while the darker zones are the amorphous domains of HDPE and SEBS matrix. The micrographs revealed the fine segregation scale and regular spacing of the HDPE domains. A tapping-mode AFM micrograph for the same blend is presented in Fig. 2d. In phase-imaging, the dark regions are the low-modulus amorphous domains, while the clear regions are the higher modulus crystalline domains. Microphase separated block copolymer morphology of SEBS phase can also be observed at higher magnification. These observations indicate good agreement between AFM and SEM morphology.

The effect of HDPE content on the morphology of HDPE/SEBS blends is presented in Fig. 3. Membranes with 30, 40, 50 and 60 wt.% HDPE were microtomed in the machine direction and observed by SEM after etching. At low HDPE content, dispersed crystalline domains revealed lamellar stack morphology elongated in the machine direction (Fig. 3a and b). As HDPE concentration was increased, elongated and twisted fibers appeared more clearly. These row-nucleated structures formed from the melt are oriented in the direction of elongation and can be clearly observed in the higher magnification insert in Fig. 3d. Each fiber had a diameter around 500 nm and consisted of a stack of 30 nm thick lamellar substructures.

Fig. 4 presents DSC melting curves for HDPE/SEBS blends. A single melting endothermal peak, associated to HDPE melting, was observed independently from the composition. A slight increase in peak area as well as in peak temperature was observed when increasing HDPE content. The endothermal peak area was normalized with regards to the HDPE content in the blends to determine the crystalline content within the HDPE phase. It was found that crystallinity increased by only 3% when the HDPE fraction was increased from 30 to 60% (Fig. 4). The melting peak was also shifted by 1.5 °C in the same composition range. This lack of significant variations indicates that the EB block of the SEBS is not interacting

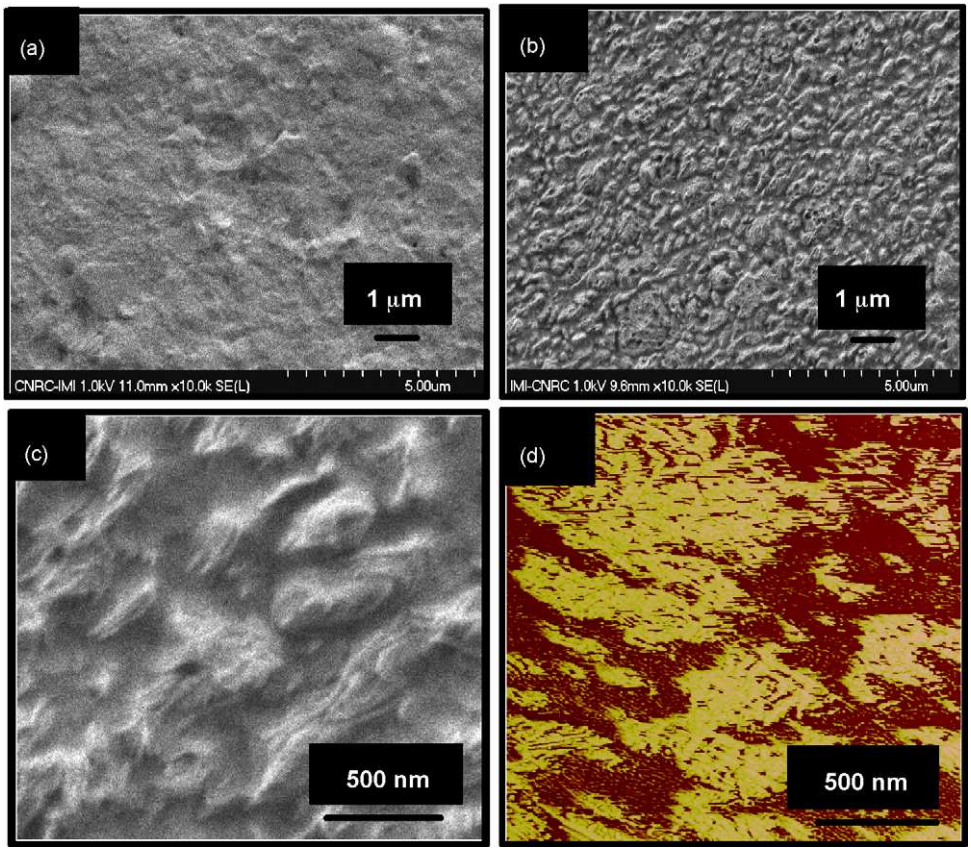

Fig. 2. Cross-sectional SEM micrograph of 50:50 SEBS/HDPE blend strand (TD) (a) freeze-fractured surface; (b) microtomed and etched surface; (c) microtomed and etched surface magnification; (d) AFM tapping mode-phase image.

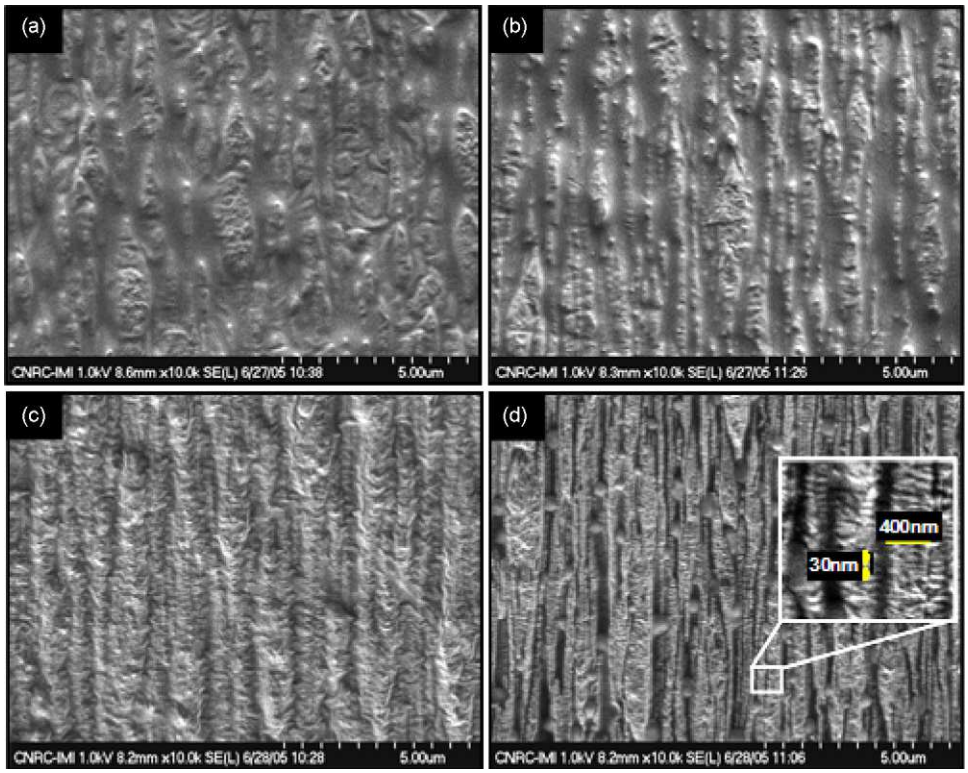

Fig. 3. SEM morphology of microtomed and etched surface for SEBS–HDPE blend membranes containing (a) 30 wt.% HDPE, (b) 40 wt.% HDPE, (c) 50 wt.% HDPE, and (d) 60 wt.% HDPE.

strongly with the HDPE phase and is not significantly interfering with HDPE crystallization.

DMTA measurements have been shown to be more sensitive than DSC for the detection of SEBS phase transitions. In Fig. 5, loss modulus E'', storage modulus E' and tan δ are plotted as a function of temperature for SEBS, HDPE and their blends. The loss modulus (Fig. 5a) exhibited a strong and narrow peak for SEBS around −50 °C which corresponds to its glass transition. For HDPE, a broader peak around 45 °C was observed. The blends presented intermediate behaviors with the difference that the first peak was shifted to a slightly higher temperature. The storage modulus (Fig. 5b) of SEBS and HDPE were also very different. The neat SEBS storage modulus dropped sharply in the −60 to −40 °C range and then stabilized up to temperatures around 80 °C. This yields a rubbery behavior over the complete range of temperature at which SEBS is typically utilized. Because of its significant crystalline fraction, the case of HDPE is quite different. The storage modulus also decreased with temperature due to the softening of the amorphous fraction but remained much higher than that of SEBS. Interestingly, all the blends exhibited a behavior that is qualitatively closer to that of SEBS in the sense that that all exhibited the sharp modulus drops around −40 °C. Thus the HDPE phase rigidified the matrix but the overall behavior of the material was still that of a thermoplastic elastomer. This further supports the fact that the SEBS was always the matrix material in the investigated concentration range, as concluded from the microscopy observations.

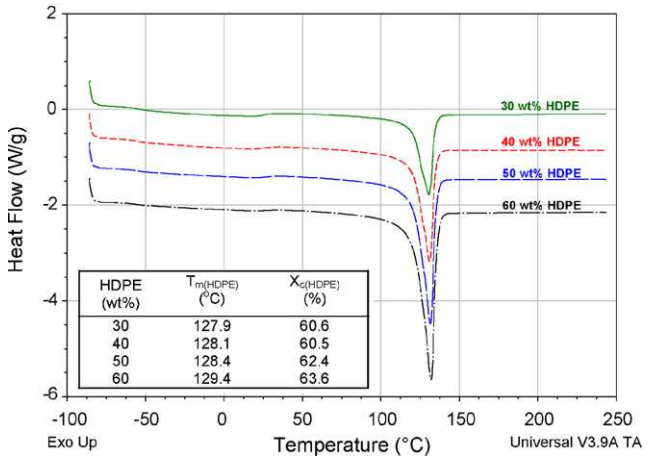

Fig. 4. DSC melting curves of HDPE/SEBS blends membranes with different HDPE contents.

The tan δ (=E''/E') measurement is often preferred to loss modulus data to determine the thermal transitions. It can be observed in Fig. 5c that all the blends clearly showed the presence of two transitions, the lower one, T_{g1}, around −40 °C is associated with the glass transition of the ethylene–butylene blocks in SEBS. The higher one, T_{g2}, around 95 °C is related to that of the styrene blocks. One relaxation peak was seen in the DMTA curves of HDPE around 70 °C, corresponding to the α relaxation [35]. This relaxation is found in all samples containing a certain degree of crystallinity, and is related to the lamellar thickness; more specifically this relaxation is due to the motion of the chains within the crystalline lamellae [35,36]. Glass transition temperatures, defined as the position of tan δ peaks are summarized in Fig. 5. The T_{g1} and T_{g2} increased by 6 and 8 °C respectively as the HDPE content was increased from 30 to 60%. T_g variations in polymer blends are common when interactions develop between the components. In this case, the relatively small variations are a sign of limited miscibility in the system.

Fig. 6 presents the tensile modulus and strain at break as a function of HDPE content. When blending a low-modulus elastomer with a stiffer HDPE material, the resulting properties will be very sensitive to the blend composition, morphology and interfacial

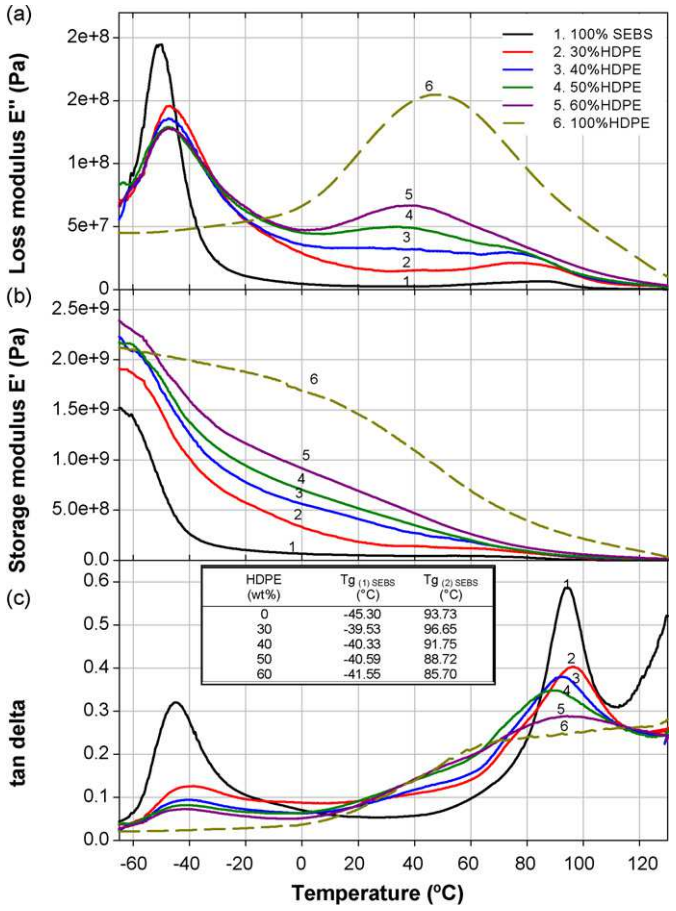

Fig. 5. Dynamic mechanical scans of HDPE/SEBS blends as a function of temperature (a) loss modulus, (b) storage modulus, and (c) tan δ.

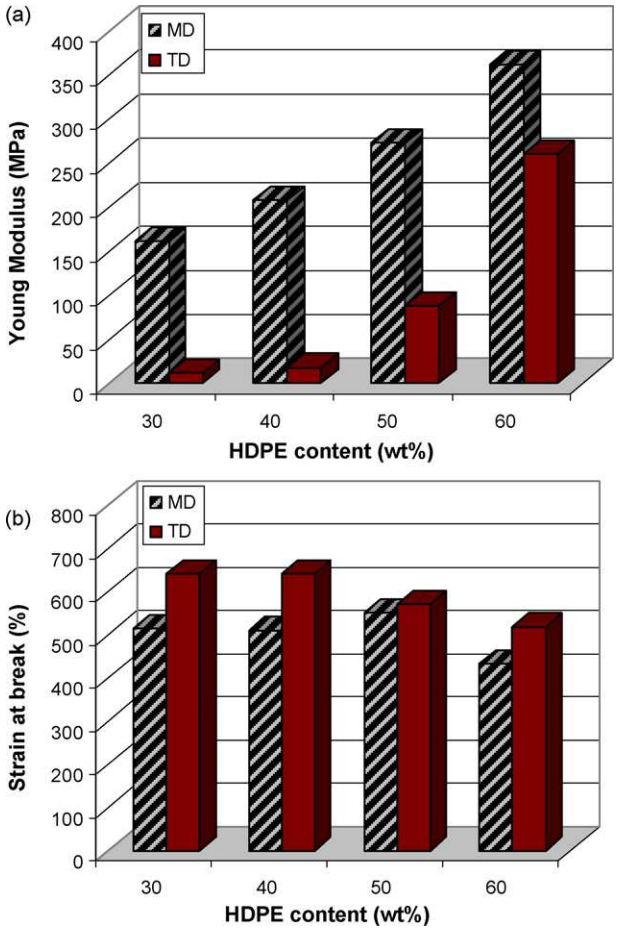

Fig. 6. Effect of HDPE content on membranes mechanical properties in the machine (MD) and transverse direction (TD) (a) Young modulus and (b) strain at break.

properties. The tensile modulus increased rapidly with HDPE content. The Young modulus in machine direction increased from 162 to 362 MPa as the HDPE concentration was raised form 30 to 60%. The tensile modulus measured in the transverse direction (TD) follows the same trend, increasing from 12 to 260 MPa, over the same concentration range. The TD values are significantly lower than those measured in MD, especially at the lower HDPE concentration. This anisotropy can be explained from changes in the blend morphology. At low HDPE concentration, the HDPE phase is expected to be mainly in the form of a nodular dispersion. When the blend is stretched during film formation, the isolated nodules are stretched into isolated fibers well oriented in the MD direction, thus significantly improving the resistance to deformation in the MD direction but not in the transverse direction. As the concentration is raised, coalescence is favored resulting in larger and a more interconnected phase (i.e. co-continuous structure). During the film formation, the preferential orientation is still given in the MD direction but due to higher continuity, the HDPE phase continues to be interconnected in the TD direction thus provided a more isotropic structure. Conversely, the strain at break decreased with HDPE concentration as expected from the stiffening of the material. The strain at break in the MD and TD direction were relatively balanced and in a very high range, above 400%, indicative of a very elastic and ductile material.

3.2. Properties of functionalized membranes

This section will focus on the functional properties most relevant to membrane applications subsequent to the film functionalization through solid-state sulfonation. One of the pre-requisite of a proton-conducting membrane is a suitable conductivity compatible with power generation requirements. In the present work, efforts were focused on the application of these proton conductors in direct methanol fuel cells operating at low temperature. In sulfonic acid-based membranes, the proton conductivity depends on the number of available acid groups and their dissociation capability in water. When the membrane is in the hydrated form, water molecules dissociate acid functionality and facilitate proton transport. Therefore, the conductivity and ionic exchange capacity are important parameters in studying PEMs. Swelling is also a key factor for the mechanical integrity of the membranes. Excessively high water uptake levels can result in dimensional changes leading to mechanical failure. These parameters have been measured for the functionalized blend series and are reported in Table 1 and compared to sulfonated SEBS and Nafion 117. Sulfonation time was varied from 60 to 120 min to assess the effect of this parameter. It was verified that the sulfonation was uniform through the membrane thickness by performing Energy Dispersive X-ray Spectrometry (EDX) along the cross-section of the membranes. All functional properties exhibited dependence on the sulfonation time and on the composition. The membrane swelling was significantly decreased by the addition of HDPE dropping from 60% for s-SEBS to around 20–30% for membranes comprising 60 wt.% HDPE. Therefore, HDPE clearly acted as a barrier reducing water uptake and swelling. Water content was much less sensitive to sulfonation time than to composition. The ionic exchange capacity was decreased significantly with HDPE content especially at the lower functionalization time of 60 min. The IEC of s-SEBS was in

Table 1
Ionic conductivity, water content and ionic exchange capacity of proton-exchange membranes at different sulfonation time.

HDPE content (wt.%)	Sulfonation time (min)	WC (%)	IEC (titr.) (meq g^{-1})	DS (%)	σ (S cm^{-1})
0		60.8	1.80	48.40	4.65E−02
30		44.9	1.42	38.10	2.59E−02
40	60	41.6	1.32	35.30	1.69E−02
50		36.0	0.71	18.99	1.38E−04
60		21.9	0.45	12.19	1.14E−04
0		62.4	1.90	50.98	6.57E−02
30		49.2	1.61	43.12	3.95E−02
40	90	44.2	1.44	38.73	2.36E−02
50		38.0	1.22	32.86	1.02E−02
60		27.2	0.74	19.97	1.90E−04
0		62.7	1.88	50.49	9.70E−02
30		49.9	1.63	43.85	4.49E−02
40	120	46.9	1.49	40.06	2.51E−02
50		39.8	1.29	34.74	1.16E−02
60		32.1	1.07	28.65	3.26E−03
Nafion 117 ref.	n/a	36.0 [40]	0.91 [40]	n/a	1.00E−02

the 1.8–1.9 meq g^{-1} range and did not increase much with sulfonation time. The blends however largely benefited from the increased treatment time. For example, at 60 wt.% HDPE, the IEC was more than doubled from 0.45 to 1.07 when the sulfonation time was increased from 60 to 120 min. In this case, it can be assumed that the HDPE is reducing the diffusion rate and thus that longer times are needed to achieve the same treatment. At 120 min of sulfonation time, all the samples present a conductivity and an IEC higher than Nafion 117 reference material, except for 60 wt.% HDPE blend which presents lower conductivity. The ionic conductivity followed similar dependencies with HDPE content and functionalization time. In this case, the obtained values were in the same range or greater than that of Nafion 117 for the pure s-SEBS and for the 30–40% HDPE blends but decreased rapidly for blends with 50% HDPE and up. This is consistent with a highest sulfonic acid content and highest degree of sulfonation, considering that HDPE is inert to sulfonation and that all conduction occurs through sulfonic acid groups grafted in styrene blocks of SEBS. Thus, high HDPE content imparts low membrane swelling but also low conductivity due to the loss of hydrophilic domain connectivity. Figs. 7 and 8 present the through-plane conductivity and water swelling of the membranes as a function of their IEC. The conductivity increased with IEC and this dependency falls on a single curve for the s-SEBS/HDPE blend series. The water uptake (Fig. 8) for all the membranes follows de same tendency and increases with increasing IEC. This indicates that the membrane properties for this blend series could be rapidly assessed through IEC measurements.

We have shown that differences in microstructure and morphology translate in differences in connectivity of the hydrophilic/hydrophobic domains. Interestingly, it is possible to find a compromise between low membrane swelling and high proton conductivity, with acceptable mechanical properties. Due to its good property balance, the 50 wt.% HDPE membrane sulfonated for 120 min was selected for further testing regarding the effect of temperature on the conductivity of the membrane. Fig. 9 presents the logarithmic plots of conductivity vs. 1000/*T*. In this plot (often referred to as the Arrhenius plot) the slope is the activation energy and is used to represent the temperature dependency. For the current membrane, the temperature dependence was evaluated at 70 and 95% relative humidity. The conductivity was higher by one order of magnitude at 95% RH and is slightly more sensitive to temperature variations. The activation energy describing the temperature dependency at 70 and 95% RH were found to be 2.1 kj/mol (0.5 kcal/mol) and 5.0 kj/mol (1.2 kcal/mol) respectively. These values are lower compared to the values reported from literature for Nafion® at 100% RH; 7.82 kj/mol (1.87 kcal/mol) from reference

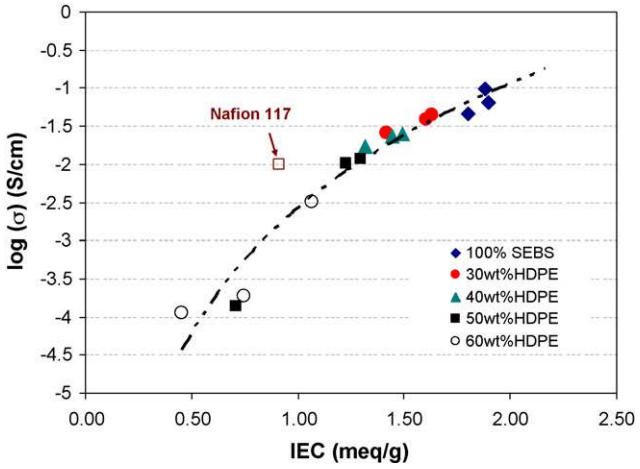

Fig. 7. Through-plane conductivity as a function of IEC for s-SEBS/HDPE blends with different HDPE contents and functionalization times at RT and 100% RH.

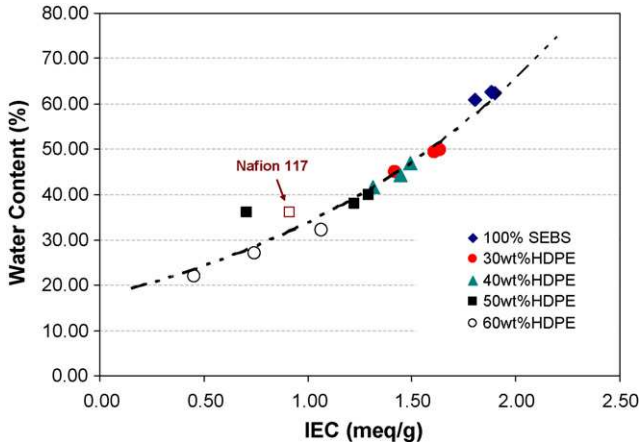

Fig. 8. Water content as a function of IEC for s-SEBS/HDPE blends with different HDPE contents and functionalization times.

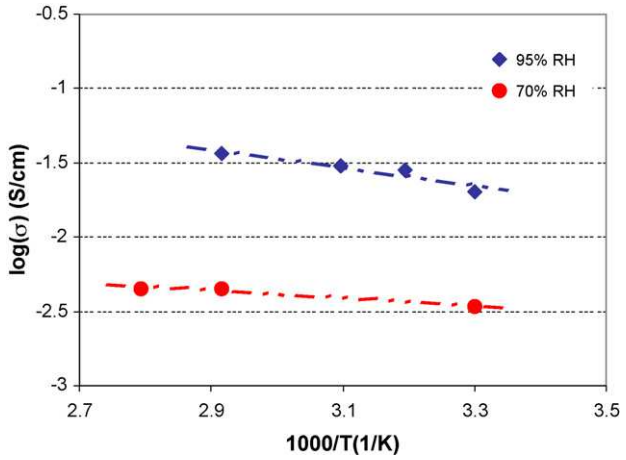

Fig. 9. Conductivity vs. temperature (Arrhenius plot) for 50% s-SEBS-120 sample at 95 and 70% relative humidity.

[37] and 9.71 kj/mol (2.32 kcal/mol) from reference [38]. The lower activation energy for the 50 wt.% HDPE membrane sulfonated for 120 min, means easier proton transfer. Since the energy barrier to proton transport decreases with increasing ion density, the higher IEC for sulfonated 50% HDPE membrane could explain this result (Table 1).

3.3. Thermal stability of composite proton-exchange membranes

The weight loss and heat flow of s-SEBS/HDPE membranes were measured in an oxygen atmosphere in a simultaneous TGA/DTA scan and are displayed in Fig. 10. The membranes sulfonated for 120 min were used for these tests. A small but gradual weight loss on heating was observed from 25 to 150 °C. The exothermal heat flow peak indicates that this was related to evaporation of small molecules such the bound water present in the membrane. It should be noted that free-water had been removed by drying under vacuum prior to the TGA/DTA analysis. The weight loss at this stage was small; 1.1 and 6.6% for 60 and 30 wt.% HDPE respectively (Table 2). As the blend membranes were heated to temperatures higher than 175 °C, there was a more important weight loss. In this case however, the weight loss was associated with a broad endothermic peak that attained its maximum value at 307 °C. This corresponds to SO_3H thermal breakdown [39]. The weight loss at this stage was

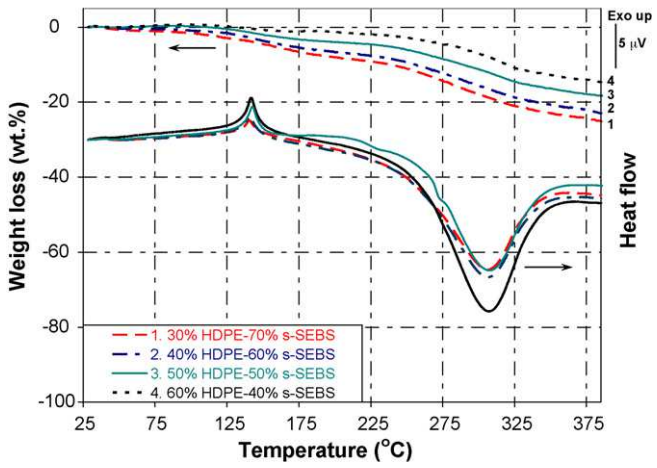

Fig. 10. Weight loss (top) and differential thermal analysis DTA traces (bottom) obtained under oxygen atmosphere for blend PEM with 120 min sulfonation time.

Table 2
Weight loss of membranes between 30 and 375 °C from TGA. The investigated membrane series was sulfonated for 120 min.

HDPE content (wt.%)	Weight loss (30–175 °C) (wt.%)	Weight loss (175–375 °C) (wt.%)	Total weight loss (30–375 °C) (wt.%)
30	6.58	17.63	24.21
40	5.43	16.68	22.11
50	3.24	14.62	17.86
60	1.13	12.87	14.00

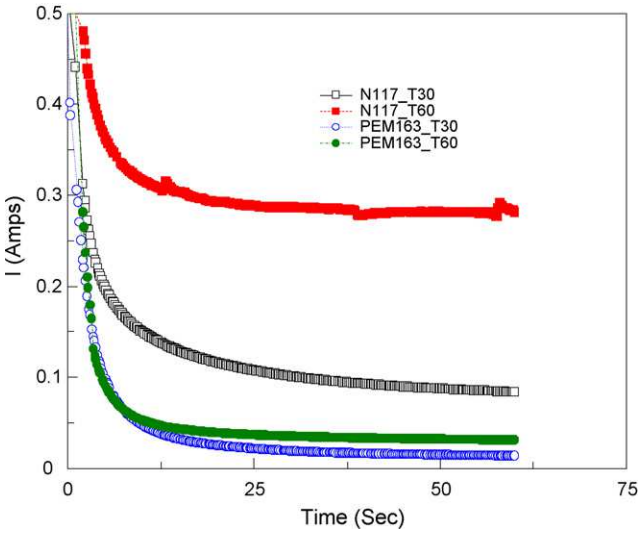

Fig. 11. In situ cyclic choronoamperometric curves measured for the oxidation of methanol permeated from anode for 50% s-SEBS-120 sample and Nafion 117 at 30 and 60 °C.

about 24% for the 30% HDPE membrane and only 14% for the 60% one.

3.4. Methanol crossover study

Methanol crossover, as shown in Fig. 11, was measured by choronoamperometry at 30 and 60 °C. The limiting currents due to methanol permeation through the s-SEBS/HDPE membrane can be qualitatively observed to be lower than through Nafion 117 at both temperatures. Methanol crossover Limited Current Densities (LCD), in units of mA cm^{-2}, are listed in Table 3 and compared to Nafion 117.

The determined LCD for s-SEBS–HDPE based membrane was 6 times lower than Nafion® at 30 °C and 15 times lower at 60 °C. It was clear that the methanol diffusion through the Nafion® membrane was considerably faster than that through the new membrane. The lower methanol permeability is also attributed to the barrier properties of crystalline structures introduced in the membrane through melt blending with HDPE.

Table 3
Activation energy as well as permeability to methanol parameters determined for 50% s-SEBS-120 sample and Nafion 117.

		50% s-SEBS-120	Nafion 117
Activation energy (kcal/mol)	At RH = 70%	0.5	1.87 at 100% RH from reference [37]
	At RH = 95%	1.2	
LCD[a] (mA cm^{-2})	T = 30 °C	2.8	16.8
	T = 60 °C	3.6	56

[a] Methanol crossover LCD (Limited Current Density) from cyclic chronoamperometry (Fig. 11).

4. Conclusions

Proton-exchange membranes were successfully produced using a blend of HDPE and sulfonated SEBS. The approach described in this work enabled the use of melt-processing technologies to form the membrane since the functionalization was carried out following the membrane melt-extrusion step. The blend morphology and tensile properties of the membrane were anisotropic due to the orientation of HDPE domains within the blend. The presence of the HDPE in the blend helped control the membrane water uptake and swelling. As expected, the membrane conductivity also decreased in presence of the HDPE but remained in an interesting range. In many cases, the through-plane conductivity of the investigated membranes surpassed that of the Nafion 117 reference materials. The best property balance was found in blends containing around 40–50 wt.% HDPE. The functionality of the blend membranes was also found to benefit more from longer sulfonation time than the pure SEBS. Therefore, further optimization of the sulfonation time as function of the membrane composition and thickness could yield even better property balances for these membranes. Methanol crossover through 50 wt.% HDPE blend membrane is found to be an order on magnitude lower than Nafion®. Therefore, the blend membranes prepared by melt processing provide a greater barrier to methanol permeability due to the morphologies generated during processing. The low methanol permeability together with the lower cost of these new hydrocarbon-based membranes present a promising alternative for widespread applications in DMFC.

Acknowledgements

The authors would like to thank K. Theberge for AFM and SEM analysis, E. Cloutier for DSC and mechanical testing, P. Sammut for DMTA, S. Mercier for TGA and M. Rodgers for the conductivity measurements. The authors would also like to thank the NRC Fuel Cell & Hydrogen Program for the financial support.

References

[1] C. Lamy, J.-M. Leger, S. Srinivasan, in: J.O.M. Bockris, B.E. Conway, R.E. White (Eds.), Modern Aspects of Electrochemistry, Kluwer Academic Publishers/Plenum Press, NY, 2001, p. 53.
[2] R. Dillon, S. Srinivasan, A.S. Aricò, V. Antonucci, International activities in DMFC R&D: status of technologies and potential applications, J. Power Sources 127 (2004) 112.
[3] K.M. McGrath, G.K.S. Prakash, G.A. Olah, Direct methanol fuel cells, J. Ind. Eng. Chem. 10 (7) (2004) 1063.
[4] V.M. Barragan, C. Ruiz-Bauza, J.P.G. Villaluenga, B. Seoane, J. Power Sources 130 (2004) 22.
[5] A. Heinzel, V.M. Barragan, J. Power Sources 84 (1999) 70.
[6] R.B. Hodgdon Jr., Polyelectrolytes prepared from perfluoroalkylaryl macromolecules, J. Polym. Sci. Part A 6 (1968) 171.
[7] R. Borup, J. Meyers, B. Pivovar, et al., Scientific aspects of polymer electrolyte fuel cell durability and degradation, Chem. Rev. 107 (2007) 3904.
[8] J.A. Horsfall, K.V. Lovell, Synthesis and characterisation of sulfonic acid-containing ion exchange membranes based on hydrocarbon and fluorocarbon polymers, Eur. Polym. J. 38 (2002) 1671.
[9] T. Hatanaka, N. Hasegawa, A. Kamiya, M. Kawasumi, Cell performances of direct methanol fuel cells with grafted membranes, Fuel 81 (2002) 2173.
[10] A.S. Aricò, V. Baglio, P. Creti, J. Schoemans, Investigation of grafted ETFE-based polymer membranes as alternative electrolyte for direct methanol fuel cells, J. Power Sources 123 (2003) 107.
[11] T. Kallio, K. Jokela, H. Ericson, F. Sundholm, Effects of a fuel cell test on the structure of irradiation grafted ion exchange membranes based on different fluoropolymers, J. Appl. Electrochem. 33 (2003) 505.
[12] M. Shen, S. Roy, J.W. Kuhlmann, K. Scott, K. Lovell, J.A. Horsfall, Grafted polymer electrolyte membrane for direct methanol fuel cells, J. Membr. Sci. 251 (2005) 121.
[13] J. Chen, M. Asano, T. Yamaki, M. Yoshida, Preparation and characterization of chemically stable polymer electrolyte membranes by radiation-induced graft copolymerization of four monomers into ETFE films, J. Membr. Sci. 269 (2006) 194.
[14] T.J. Schmidt, K. Simbeck, G.G. Scherer, Influence of cross-linking on performance of radiation-grafted and sulfonated FEP 25 membranes in H_2–O_2 PEFC, J. Electrochem. Soc. 152 (2005) A93.
[15] G. Alberti, M. Casciola, Composite membranes for medium temperature fuel cells, Annu. Rev. Mater. Res. 33 (2003) 129.
[16] H.Y. Chang, C.W. Lin, Proton conducting membranes based on PEG/SiO_2 nanocomposites for direct methanol fuel cell, J. Membr. Sci. 218 (2003) 295.
[17] V. Baglio, A. Di Blasi, A.S. Aricò, V. Antonucci, P.L. Antonucci, C. Trakanprapai, V. Esposito, S. Licoccia, E. Traversab, Composite mesoporous titania Nafion-based membranes for direct methanol fuel cell operation at high temperature, J. Electrochem. Soc. 152 (7) (2005) A1373.
[18] J.M. Thomassin, C. Pagnoulle, G. Caldarella, A. Germain, R. Jérôme, Contribution of nanoclays to the barrier properties of a model proton exchange membrane for fuel cell application, J. Membr. Sci. 270 (2006) 50.
[19] A.M. Herring, Inorganic-polymer composite membranes for proton exchange membrane fuel cells, J. Mol. Sci. Part C Polym. Rev. 46 (2006) 245.
[20] G. Alberti, M. Casciola, Layered metallic phosphonates, a large class of inorganic–organic proton conductors, Solid State Ionics 97 (1997) 177.
[21] R. Wycisk, J. Chisholm, J. Lee, J. Lin, P.N. Pintauro, Direct methanol fuel cell membranes from Nafion–polybenzimidazole blends, J. Power Sources 163 (2006) 9.
[22] J.C. Lin, M. Ouyang, J.M. Fenton, H.R. Kunz, J.T. Koberstein, M.B. Cutlip, Study of blend membranes consisting of Nafion and vinylidene fluoride–hexafluoropropylene copolymer, J. Appl. Polym. Sci. 70 (1998) 121.
[23] A. Mokrini, J.L. Acosta, Studies of sulfonated block copolymer and its blends, Polymer 42 (2001) 9.
[24] A. Mokrini, M.A. Huneault, Proton exchange membranes based on PVDF/SEBS blends, J. Power Sources 154 (2006) 51.
[25] A. Mokrini, M.A. Huneault, P. Gerard, Partially fluorinated proton exchange membranes based on PVDF–SEBS blends compatibilized with methyl methacrylate based block copolymers, J. Membr. Sci. 283 (1–2) (2006) 74.
[26] P.Y. Vuillaume, A. Mokrini, K. Théberge, L. Robitaille. Heteropolyacid/saponite-like clay complexes and their blends in amphiphilic SEBS, J. Mater. Chem., submitted for publication.
[27] S.G. Ehrenberg, J.M. Serpico, B.M. Sheikh-Ali, T.N. Tangredi, E. Zador, G.E. Wnek, in: O. Savadogo, P.R. Roberge (Eds.), Proceedings of the Second International Symposium on New Materials for Fuel Cell and Modern Battery Systems, Montreal, Canada, 6–10 July, 1997, p. 828.
[28] S.G. Ehrenberg, J.K. Serpico, G.E. Wnek, J.N. Rider, Fuel cell incorporating novel ion-conducting membrane, US Patent, 5,468,574 (1995).
[29] A. Mokrini, C. Del Rio, J.L. Acosta, Synthesis and characterization of new ion conductors based on butadiene styrene copolymers, Solid State Ionics 166 (2004) 375.
[30] A. Mokrini, J.L. Acosta, Comparative study of polymer single cells based on sulfonated linear and star butadiene–styrene block copolymer electrolyte membranes, J. Appl. Polym. Sci. 83 (2002) 367.
[31] A. Mokrini, J.L. Acosta, New ion conducting systems based on star branched block copolymer, Polymer 42 (2001) 8817.
[32] G.E. Wnek, J.N. Rider, J.M. Serpico, A.G. Einset, Proceedings of the First International Symposium on Proton Conducting Membrane Fuel Cells, Electrochemical Society Proc., 1995, p. 247.
[33] J. Won, S.W. Choi, Y.S. Kang, H.Y. Ha, I.H. Oh, H.S. Kim, K.T. Kim, W.H. Jo, Structural characterization and surface modification of sulfonated polystyrene–(ethylene–butylene)–styrene triblock proton exchange membranes, J. Membr. Sci. 214 (2003) 245.
[34] R.H. Olley, A.M. Hodge, D.C. Bassett, J.J. Thomson, A permanganic etchant for polyolefines, J. Polym. Sci.: Polym. Phys. 17 (1979) 627.
[35] M. Munaro, L. Akcelrud, Correlations between composition and crystallinity of LDPE/HDPE blends, J. Polym. Res. 15 (2008) 83.
[36] N. Alberola, J.Y. Cavaille, J. Perez, Mechanical spectrometry of alpha-relaxations of high-density polyethylene, J. Polym. Sci. B Polym. Phys. 28 (1990) 569.
[37] R.W. Kopitzke, C.A. Linkous, H.R. Anderson, G.L. Nelson, Conductivity and water uptake of aromatic-based proton exchange membrane electrolytes, J. Electrochem. Soc. 147 (5) (2000) 1677.
[38] F. Lufrano, I. Gatto, P. Staiti, V. Antonucci, E. Passalacqua, Sulfonated polysulfone ionomer membranes for fuel cells, Solid State Ionics 145 (2001) 47.
[39] M. Matsuda, K. Funabashi, Influence of functional sulfonic acid groups on styrene–divinylbenzene copolymer pyrolysis, J. Polym. Sci. Part A: Polym. Chem. 25 (2) (2003) 669.
[40] T.A. Zawodzinski, C. Derouin, S. Radzinski, R.J. Sherman, V.T. Smith, T.E. Springer, S. Gottesfeld, Water uptake by and transport through Nafion 117 membranes, J. Electrochem. Soc. 140 (4) (1993) 1041.